JACS
JOURNAL OF THE AMERICAN CHEMICAL SOCIETY
pubs.acs.org/JACS
Article

Integrated Carbon Dioxide Capture by Amines and Conversion to Methane on Single-Atom Nickel Catalysts

Tomaz Neves-Garcia, Mahmudul Hasan, Quansong Zhu, Jing Li, Zhan Jiang, Yongye Liang, Hailiang Wang,* Liane M. Rossi,* Robert E. Warburton,* and L. Robert Baker*

Cite This: J. Am. Chem. Soc. 2024, 146, 31633−31646
Read Online

ABSTRACT: Direct electrochemical reduction of carbon dioxide (CO_2) capture species, i.e., carbamate and (bi)carbonate, can be promising for CO_2 capture and conversion from point-source, where the energetically demanding stripping step is bypassed. Here, we describe a class of atomically dispersed nickel (Ni) catalysts electrodeposited on various electrode surfaces that are shown to directly convert captured CO_2 to methane (CH_4). A detailed study employing X-ray photoelectron spectroscopy (XPS) and electron microscopy (EM) indicate that highly dispersed Ni atoms are uniquely active for converting capture species to CH_4, and the activity of single-atom Ni is confirmed using control experiments with a molecularly defined Ni phthalocyanine catalyst supported on carbon nanotubes. Comparing the kinetics of various capture solutions obtained from hydroxide, ammonia, primary, secondary, and tertiary amines provide evidence that carbamate, rather than (bi)carbonate and/or dissolved CO_2, is primarily responsible for CH_4 production. This conclusion is supported by ^{13}C nuclear magnetic resonance (NMR) spectroscopy of capture solutions as well as control experiments comparing reaction selectivity with and without CO_2 purging. These findings are understood with the help of density functional theory (DFT) calculations showing that single-atom nickel (Ni) dispersed on gold (Au) is active for the direct reduction of carbamate, producing CH_4 as the primary product. This is the first example of direct electrochemical conversion of carbamate to CH_4, and the mechanism of this process provides new insight on the potential for integrated capture and conversion of CO_2 directly to hydrocarbons.

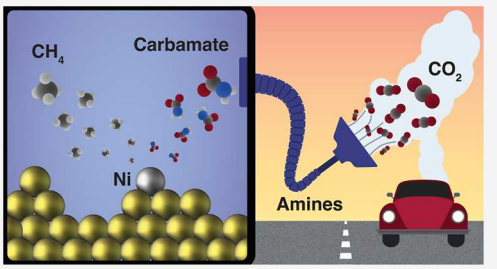

INTRODUCTION

Developing technologies to efficiently capture and convert carbon dioxide (CO_2) to products of interest has potential to mitigate the environmental consequences of this greenhouse gas while also providing renewable paths to produce carbon-based molecules, including fuels, that are currently derived from nonrenewable, petroleum sources.[1−3] One of the most significant challenges associated with CO_2 utilization is the need to capture and sequester this molecule from air or from point of source production, and the energy costs associated with CO_2 capture currently make this process unviable for commercial CO_2 utilization.[4] For example, amine-based capture solutions are highly efficient for converting CO_2 to carbamate; however, the subsequent release of CO_2 to regenerate the amine requires significant energy,[5−7] consuming up to one-third the total energy produced from fossil fuel combustion.[8] Due to the high activation barrier associated with electrochemical CO_2 reduction, additional energy is further lost during conversion of CO_2 to products.[9] Accordingly, CO_2 capture followed by electrochemical CO_2 conversion represents two energy intensive processes that must proceed in sequence. One approach to improving the overall efficiency of CO_2 capture and utilization (CCU) is instead to integrate the capture and conversion processes via the direct electrochemical reduction of the capture solution.[10−19] This integrated approach allows for conversion of CO_2 and regeneration of the capture species in a single step, completely eliminating the energy loss associated with the release of CO_2 from capture solutions.[11−18] Despite the importance of closing the carbon (C) cycle, to date there are no examples of an electrocatalyst capable of converting the CO_2 capture species, carbamate, directly to a hydrocarbon. Understanding the mechanism of a catalyst capable of such a process would open the door to rational design of new material platforms capable of direct conversion of CO_2 capture solutions to alternative fuels or other value-added products.

The capture medium, usually a 30% monoethanolamine (MEOA) saturated with CO_2, can be employed as the electrolyte for the direct electrochemical conversion of excess CO_2 purged prior the electrolysis.[20] This approach was followed by other studies where single-atom nickel (Ni)

Received: July 19, 2024
Revised: October 29, 2024
Accepted: October 29, 2024
Published: November 6, 2024

https://doi.org/10.1021/jacs.4c09744
J. Am. Chem. Soc. 2024, 146, 31633−31646

directly converted captured CO_2 to carbon monoxide (CO).[21] Additionally, coinage metals, i.e. gold (Au), silver (Ag) and copper (Cu), with nanodendrite structures have been shown to convert CO_2 to formate[22] also using the amine capture medium as the electrolyte. However, the presence of amines in the performance of the direct CO_2 reduction in some cases can be detrimental. The presence of ammonium cations can block the surface from CO_2 under negative bias,[23] and similar to bicarbonate may serve as a proton donor,[24] increasing the competing hydrogen evolution reaction (HER).[23,25−29] Additionally, an increase in the catalyst corrosion and reconstruction was observed in the presence of amine-CO_2 capture species.[25] Therefore, the development of electrolyzers and new catalysts to directly convert carbamate to different CO_2 reduction products remains important for integrated CO_2 capture and electrochemical reduction.[10] Direct carbamate conversion was studied on a copper (Cu) electrode, and 58% FE toward CO was observed at 18.4 mA cm^{-2} with ethylenediamine (EDA) as the capture agent.[30] However, in this study the presence of carbamate was demonstrated in absence of water, while the reactions were performed in aqueous solution. Sargent and co-workers studied the carbamate conversion using silver (Ag) nanoparticles supported on a sputtered Ag film catalysts, where 72% FE at 50 mA cm^{-2} were achieved toward CO with MEOA at 60 °C.[31] This study specifically demonstrated that tailoring the electrical double layer (EDL) with small cations is imperative to bring the negatively charged carbamate species to the negatively charged surface. Contrasting studies[25−27] using Ag film, suggested that at 60 °C free CO_2 is present and may be the source of products.

Although the concentration of capture species is often much higher than dissolved CO_2,[32] in some cases it can be difficult to determine whether the observed product is the result of carbamate reduction or reduction of free CO_2 that persists in the electrolyte due to slow equilibration.[21,25−27,33] Most lab-based capture solutions are prepared by purging CO_2 in an aqueous amine solution for an extended time resulting in a distribution of free CO_2, bicarbonate, carbonate, and carbamate. In contrast, CO_2 capture in an industrial setting involves a short interaction time of amine solutions with CO_2 resulting in the kinetically favored carbamate product with only small amounts of free CO_2.[34] A number of studies have shown that conversion of free CO_2 is significantly more active than direct carbamate conversion,[21,23,25−27] and care must be taken to differentiate between these two pathways because catalysts that show high activity for conversion of dissolved CO_2 may not be active for conversion of a capture solution containing primarily carbamate. While a number of catalysts show activity for reduction of an amine-based capture solution,[13,20−23,25−27,30−32,35−38] there are only a handful of materials that are active for direct carbamate conversion, and to date there are no reports of a catalyst that is capable of producing hydrocarbons directly from carbamate.

In this study we show that a single-atom Ni catalyst dispersed on various conductive electrode materials can reduce an amine capture solution directly to methane (CH_4). We observe a distribution of CO and CH_4 as the only two C-containing products, with certain single-atom Ni catalysts impressively showing a higher selectivity to CH_4 than to CO. Systematically comparing the results for captures solutions based on ammonia (NH_3), monoethylamine (MEA), and diethylamine (DEA), which are capable of forming carbamate, with triethylamine (TEA), which as a tertiary amine is not capable of producing carbamate, we provide strong evidence that CH_4 is the result of direct carbamate reduction and does not depend on the presence of free CO_2. This conclusion is further supported by time-dependent kinetic measurements of a molecular nickel phthalocyanine catalyst supported on carbon nanotubes (NiPc-OMe@CNT) showing that CO production is extremely sensitive to the concentration of dissolved CO_2, while CH_4 production is not. Finally, density functional theory (DFT) calculations identify a novel reaction mechanism for selectively breaking the C−N bond of the carbamate intermediate on Ni single-atoms. Together these findings represent the first report of direct carbamate conversion to CH_4 and provide key mechanistic insight necessary to guide the design of catalytic systems for integrated CO_2 capture and conversion.

RESULTS AND DISCUSSION

Figures 1a,b and S1 show the results of electrochemical reduction of various CO_2 capture solutions using a polycrystal-

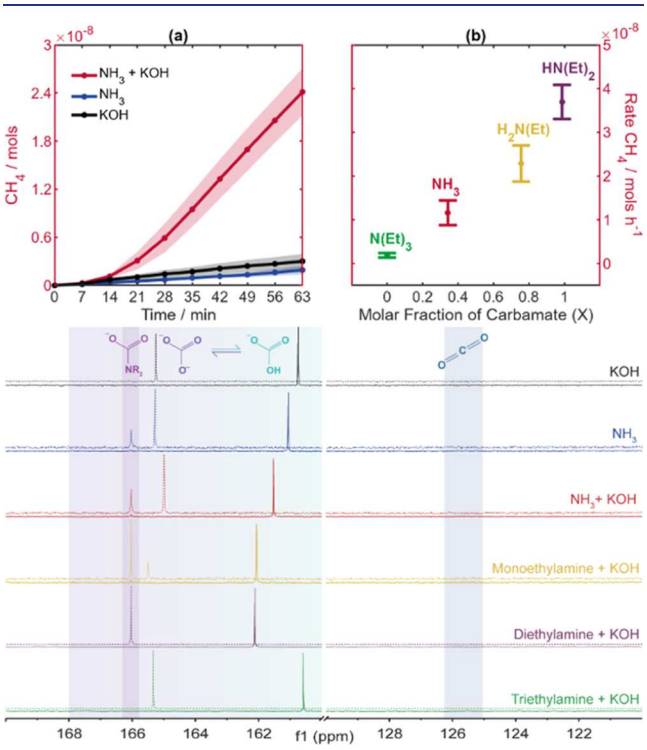

Figure 1. Reduction of CO_2 capture species on a polycrystalline gold (Au) surface with no previous treatment. The kinetics experiments were performed at −1.5 V vs silver/silver chloride reference electrode (Ag/AgCl) for 63 min. The solutions were prepared by capturing CO_2 by 0.5 M of NH_3 and/or 0.5 M KOH followed by N_2 purging (a). Results are also compared for capture solutions of 0.5 M NH_3, MEA, DEA, or TEA each with 0.5 M KOH (b). The NMR spectra show the species present in solution after the capture by all the capture agents (solid line) and after the capture at pH 10 (dashed lines) (c).

line Au electrode, and Figure 1c shows the corresponding ^{13}C nuclear magnetic resonance (NMR) spectra of the capture solutions. The corresponding ^{1}H NMR of each amine capture solution can be found in Figure S2 in the Supporting Information. In these experiments, each solution is purged with CO_2 for 30 min followed by purging with nitrogen (N_2)

https://doi.org/10.1021/jacs.4c09744
J. Am. Chem. Soc. 2024, 146, 31633−31646

for 30 min to remove the majority of dissolved CO_2 from solution. Kinetic results from electrochemical reduction of three capture solutions are shown in Figures 1a and S1a,b of the Supporting Information: (1) potassium hydroxide (KOH) (0.5 M), (2) NH_3 (0.5 M), and the combination of KOH and NH_3 (0.5 M each). Note that hydroxide solutions as well as amine solutions capture free CO_2 yielding bicarbonate as the capture species[39−50] as shown in the equations.

$$CO_2 + OH^- \rightleftharpoons HCO_3^- \quad (1)$$

$$NH_3 + CO_2 + H_2O \rightleftharpoons HCO_3^- + NH_4^+ \quad (2)$$

Because bicarbonate exists in equilibrium with carbonate, we refer to this mixture of species simply as (bi)carbonate. Additionally, CO_2 can react with an amine to form a zwitterionic intermediate (eq 3) that reacts with a second amine to produce carbamate (eq 4).[39−50]

$$CO_2 + NH_3 \rightleftharpoons H_3N^+CO_2^- \quad (3)$$

$$H_3N^+CO_2^- + NH_3 \rightleftharpoons H_2NCO_2^- + NH_4^+ \quad (4)$$

Considering the distribution of species that can be present in the capture solution, Figure 1a shows the CH_4 yield vs time for electrochemical reduction of the three capture solutions. Interestingly, only the third capture solution consisting of both KOH and NH_3 shows a significant amount of CH_4 production, while individual solutions of only KOH or NH_3 show very low CH_4 yield by comparison. Corresponding yields for CO and H_2 are given in Figure S1. This result raises two questions: First, what is the origin of the CH_4, or in other words, what capture species is being reduced? Second, what is the active catalyst for this transformation, given that Au is considered a selective catalyst for CO formation and is not expected to produce CH_4? To consider the first question, we examine the ^{13}C NMR spectra. The solid lines in Figure 1c show the ^{13}C spectra obtained immediately following CO_2 and N_2 purging. First, we observe the absence of the free $^{13}CO_2$ peak at 125.5 ppm in all spectra; however, as has been shown previously, we cannot exclude that small amounts of free CO_2 may still be present during reaction and contribute to the observed reaction kinetics. Second, we observe that the majority of captured CO_2 exists as (bi)carbonate. This is evident by the peaks present between 160 and 168 ppm representing the fast equilibrium between carbonate and bicarbonate.[45]

Given the similar concentration of (bi)carbonate in each of the three capture solutions, conversion of this species cannot explain the relatively high yield of CH_4 only from the KOH + NH_3 capture solution. Rather, this behavior can be understood by attributing the carbamate species as the active species to produce methane. Unlike (bi)carbonate, carbamate is only formed when an amine is present in the capture solution. However, as described by Sargent and co-workers,[31] the negatively charged carbamate is separated from the negatively charged surface by the large ammonium cation. Tailoring the electric double layer (EDL) by addition of small alkaline metal cations is required to bring the carbamate closer to the surface to be reduced. Therefore, the results showed in Figure 1a are nicely explained by the fact that the negatively charged carbamate is only formed when NH_3 is present but can only be reduced at the negatively charged surface when a small cation, such as K^+, is present in the EDL.

To evaluate whether the increased rate of CH_4 production in the presence of KOH is primarily a result of the inorganic base or is due to the presence of K^+ in the supporting electrolyte, we have measured kinetics for electrolyte solutions where KCl was added to the electrolyte instead of KOH. In this case, we observe a similar rate for CH_4 production even though KCl is not a base (see Figure S1 in the Supporting Information). This indicates that the primary mechanism for CH_4 rate enhancement upon addition of KOH (or KCl) is due to the presence of an alkali cation that is able to bring carbamate to the electrode surface as shown previously.[31] Figure S1 also shows the pH of the different capture solutions before and after CO_2 purging. Although the initial values differ, each capture solution equilibrates to a nearly identical pH of 8.2 following CO_2 purging, indicating that there are no significant differences in pH of the capture solutions during electrolysis.

Because carbamate is favored at basic pH,[40−44] the dashed lines in Figure 1c show the ^{13}C NMR spectrum for each of the capture solutions following the addition of excess KOH added after the CO_2 and N_2 purging steps to achieve a pH close to 10. Because the additional KOH is added after purging the solutions, this does not change the total amount of CO_2 captured; rather, it only shifts the equilibrium between the capture species. As shown in the dashed lines in Figure 1c, increasing the pH shifts the (bi)carbonate equilibrium toward carbamate, which is seen as a significant increase in the peak around 166 ppm. We note that under cathodic reaction conditions, a pH gradient is expected near the electrode surface due to production of OH^- from the various reduction reactions,[51−53] including HER shown in Figure S1. As seen in Figure 1c, the resulting pH gradient will tend to shift the equilibrium of the capture species toward carbamate, near the electrode surface. This is illustrated in Figure S3, which shows the relative speciation of (bi)carbonate and carbamate as a function of pH obtained by solving the coupled equilibrium equations.

To confirm whether the formation of carbamate near the electrode surface plays a role in the observed production of CH_4, the same reaction was carried out for an additional series of capture solutions to compare results for NH_3, monoethylamine (MEA), diethylamine (DEA), and triethylamine (TEA). Each of these amines is capable of capturing CO_2 to (bi)carbonate as shown in eq 2. In contrast, tertiary amines, such as TEA, are unable to produce carbamate according to eq 4. Consequently, while carbamate will be present in NH_3, MEA, and DEA capture solutions, it will be absent from the TEA solution. This is confirmed in Figure 1c, which shows that while (bi)carbonate is observed in every capture solution, carbamate is only observed in NH_3, MEA, and DEA capture solutions but is absent in TEA. Results of the electrochemical reduction reactions for each capture solution are shown in Figure 1b.

Using ^{13}C NMR from Figure 1c, it is possible to quantify the carbamate mole fraction defined as the ratio of carbamate:(bi)carbonate concentrations, which increases with increasing number of ethyl groups. TEA represents the only exception because tertiary amines are unable to produce carbamate. Plotting the rate of CH_4 production as a function of carbamate mole fraction reveals a direct correlation indicating that CH_4 production increases with increasing carbamate concentration. This finding suggests that carbamate is primarily responsible for production of CH_4. Additional control experiments to observe the effect of dissolved CO_2 on CH_4 yield is described

https://doi.org/10.1021/jacs.4c09744
J. Am. Chem. Soc. 2024, 146, 31633−31646

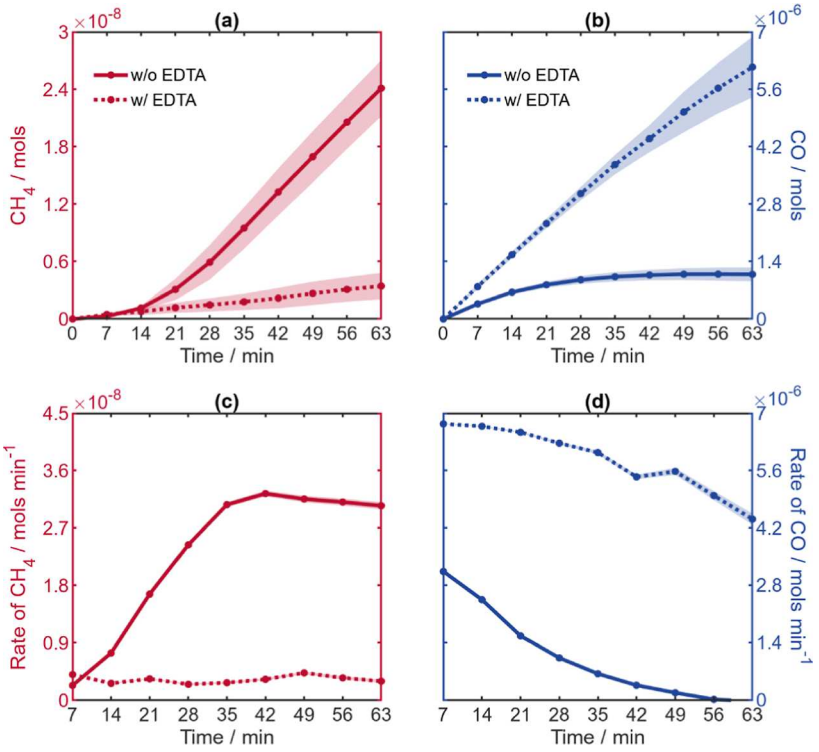

Figure 2. Reduction of CO_2 capture species on a polycrystalline gold (Au) surface with and without previous treatment with EDTA, yielding CH_4 (a) and CO (b). The kinetics experiments were performed at −1.5 V vs Ag/AgCl for 63 min. The solutions were prepared by capturing CO_2 by 0.5 M of NH_3 and 0.5 M of KOH. To better visualization the obtained data was also plotted as rate of CO production (c) and rate of CH_4 production (d).

further below. It is worth noting that ^{1}H NMR shows no byproducts associated with amine degradation following reaction of the capture solution (see Figure S4 in the Supporting Information).

However, we should first consider that the actual active site for CH_4 production is unknown, and that Au is not expected to yield hydrocarbon products from either CO_2 or carbamate. To obtain insights on the catalyst active site, we note that in these experiments on Au electrodes, the formation of CO was also detected with significantly higher selectivity compared to CH_4 as shown in Figure S1. CO is also observed when KOH and NH_3 are employed alone and in the TEA capture solution, suggesting that CO is produced primarily from the (bi)-carbonate species. However, a strong deactivation is observed for CO production, and after 1 h of reaction, the CO formation is completely shut off, while CH_4 formation persists with no sign of deactivation. It is known that trace transition metals impurities will deposit on Au active sites during CO_2 reduction, and this process causes rapid deactivation of CO formation.[54−57] Several strategies exist to prevent electro-deposition of trace metal impurities; these include careful electrolyte purification,[58] addition of chelating agents to bind trace metals,[54,55,58,59] and operating the electrocatalyst in the presence of hydrophobic surface ligands, which hinders electrodeposition of metal ions.[60] Transition metal impurities are commonly present in electrolyte salts, and even the purest salts commercially available are contaminated with trace impurities.[58,61]

To study the influence of trace metals deposition on Au electrodes on the conversion of CO_2 capture species, additional experiments were performed where the capture solution was treated with ethylenediaminetetraacetic acid (EDTA) prior to the capture and conversion reactions. EDTA is known to efficiently chelate transition metals and prevent their deposition on the electrode surface under a negative bias. Figure 2a,b shows that in the presence of EDTA the time dependent reactivity presents a reversed trend. CO production shows a significantly reduced deactivation over 1 h of reaction. This indicates that EDTA effectively prevents the deposition of trace metals on the Au active sites. In contrast, the CH_4 production on Au is significantly reduced and remains close to zero throughout the 1 h reaction. These observations can be better visualized when the rate of product formation is plotted rather than the accumulated number of moles (Figure 2c,d). In the absence of EDTA the rate of CO formation drops to zero within 1 h, whereas the rate of CH_4 increases steeply, reaching a maximum within 42 min. In contrast, in the presence of EDTA, the rate of CH_4 remains near zero and the rate of CO only drops slightly. These results suggest that the deposition of trace transition metals, present as intrinsic impurities even in high purity electrolyte salts, are responsible for promoting the observed CH_4 formation. To understand the conversion of CO_2 capture species to CH_4 it is necessary to identify the specific metal(s) responsible for this reaction, and investigate the role of the Au electrode, if any, to facilitate the observed electrocatalysis.

To identify and quantify the metals deposited on the surface, X-ray photoelectron spectroscopy (XPS) was performed to characterize the Au electrode surface following electrochemical reduction reactions in the presence and absence of EDTA. As shown in Figure 2, following 42 min of reaction we observe the maximum rate of methane production, so the characterization of the surface at this time provides a good understanding of the surface composition responsible for methane formation. The

https://doi.org/10.1021/jacs.4c09744
J. Am. Chem. Soc. 2024, 146, 31633−31646

survey spectrum, as well as the high-resolution spectra of each expected metal present in the electrolyte were measured for both samples. The survey spectrum is shown in Figure S5 of the Supporting Information, and Figure 3 shows the high-resolution spectra for each of the metals detected. Except for Al, all the metals present as contaminants in the KOH electrolyte (Ensure, Sigma-Aldrich) were observed on the electrode surface: Fe, Ni, Cu, Zn and Pb. No metals other than these were detected in the XPS experiment, suggesting that this is the primary source of trace metals deposited on the electrode surface during reaction. In contrast, the characterization of the surface after the reaction in the presence of EDTA showed no detectable signal for any metal other than Au (dashed lines), indicating that the Au electrode is not contaminated during reaction with EDTA.

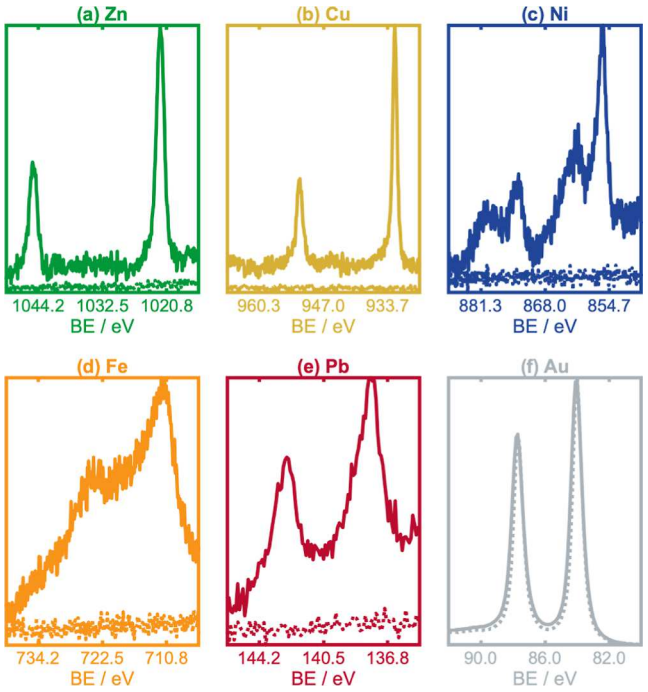

Figure 3. X-ray photoelectron spectroscopy (XPS) of the gold electrode after the reaction performed with (dashed line) and without (solid line) the EDTA treatment prior to the experiment.

The details of the calculation can be found in Section S3 of the Supporting Information, and the obtained results are shown in Table 1.

To determine which metal or combination of metals is responsible for CH_4 production, we performed controlled, selective deposition of each metal individually on the Au surface starting from a purified electrolyte, and then evaluated the electrocatalytic activity of each surface. To accomplish the selective metal deposition, EDTA (3.2 μM) was added to the reaction solution before the capture process, so all the metallic contaminants from the electrolyte are chelated and prevented from depositing on the electrode surface. After addition of EDTA but immediately before the electrocatalytic reaction, an excess of the desired metal salt was added (10 μM). The low lability of the EDTA-transition metal complex prevents the exchange of ligand among the metals in solution and assures the selective deposition of the desired metal. Figure 4a–f shows the XPS spectra for the selective deposition experiments. As shown, in each case only the desired metal ion deposits on the Au surface.

Electrocatalytic reduction of the carbamate-containing capture solution was performed using the Au electrodes prepared by selective deposition of each of the respective transition metal ion impurities. Figure 4g,h show the formation of CH_4 and CO, respectively, for these experiments. In the presence of any of the tested metals, the CO formation is shut off completely, showing that deposition of each of these metals completely blocks the active sites responsible for CO production on Au. Although each of the metals has an influence on the CO production kinetics, only Ni shows activity for methane production. The rate of methane formation obtained from Ni selectively deposited on Au (Ni@Au) was indentical to the maximum rate observed for the untreated, impure electrolyte, although there was no initial induction period (see Figure S6 at the Supporting Information). This shows that at higher electrolyte concentration Ni rapidly deposits on Au giving rise to greater CH_4 production during the early time of the reaction although the final rate after 1 h is nearly identical. This result demonstrates that Ni deposited on Au (Ni@Au) is the active species for the formation of CH_4 from the amine-based capture solutions. These kinetics also suggest that after deposition of a small amount of Ni at the surface ($\leq$5.74% of a monolayer) the deposition of additional Ni does not further promote the reaction indicating that highly dispersed Ni atoms on the gold electrode are responsible for the turnover of carbamate to CH_4. Given the quantitatively measured Ni surface coverage determined by XPS (Table 1) and the corresponding rate of CH_4 formation measured at 42 min of reaction it is possible to estimate a lower limit for the turnover frequency of the Ni@Au catalyst. The details of the calculations can be found in Section S3 of the Supporting Information. From this analysis we found a turnover frequency of $\geq$38 $\pm$ 1.6 mmol (CH_4) mol^{-1} (Ni) s^{-1}. This rate of formation was stable for more than 6 h, and the yield of CH_4 was the same following 1 week of storage of the capture solution, as shown in Figure S7 of the Supporting Information.

To evaluate whether the gold substrate plays any role in the production of CH_4 or if Ni alone is responsible for the observed activity, the reaction was performed using Ni selectively deposited on various electrodes in addition to Au. Figure 5 compares the CO and CH_4 cumulative production and the associated time-dependent rate for Ni deposited on Au (Ni@Au), Cu (Ni@Cu), glassy carbon (Ni@GC), and a pure Ni electrode (Ni). First, we note that the CO production is nearly zero for all catalysts tested, with the exception only of Ni@Au. Au is a known catalyst for CO formation, and as such showed a brief period of CO production that completely

Table 1. Quantification of Trace Metal Deposition on Au during Electrolysis

	aluminum (Al)	iron (Fe)	nickel (Ni)	cupper (Cu)	zinc (Zn)	lead (Pb)
atomic fraction/%	<LOD	4.76	3.78	3.74	2.71	0.45
surface coverage/%	<LOD	7.23 $\pm$ 0.30	5.74 $\pm$ 0.24	5.68 $\pm$ 0.24	4.12 $\pm$ 0.18	0.68 $\pm$ 0.03

https://doi.org/10.1021/jacs.4c09744
J. Am. Chem. Soc. 2024, 146, 31633–31646

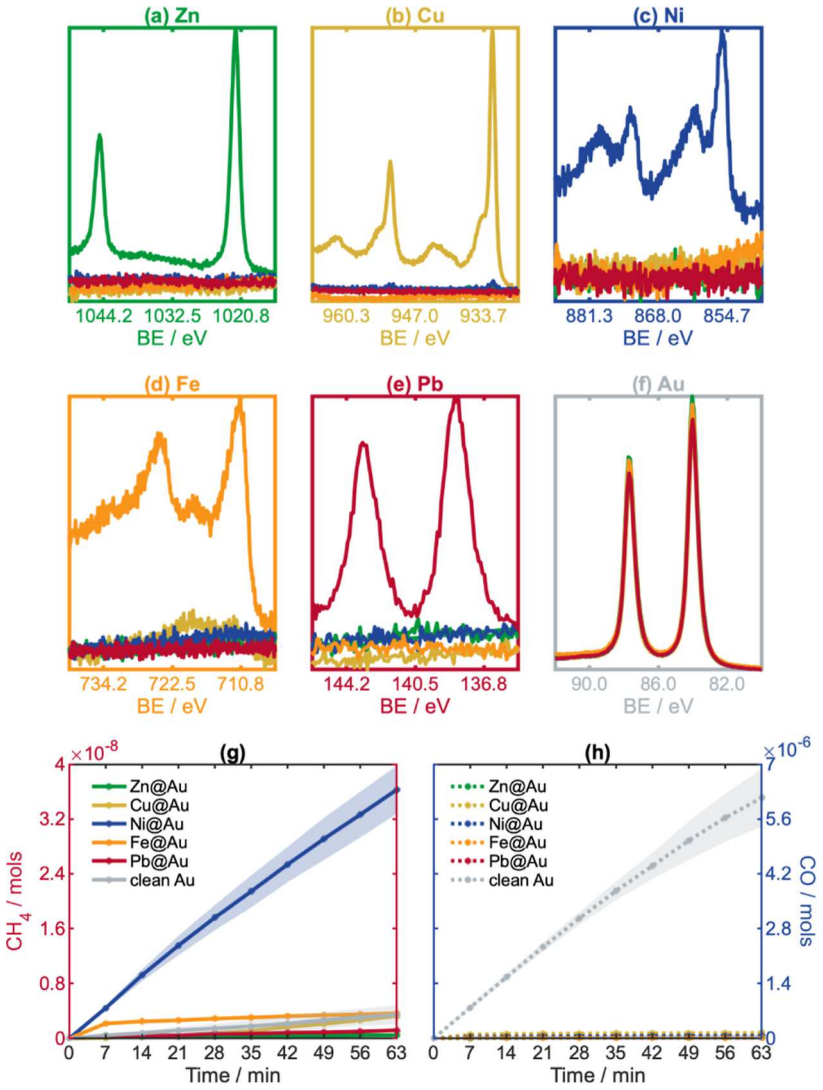

Figure 4. X-ray photoelectron spectroscopy (XPS) of the gold electrode after the selective deposition of each metal (a–f) and Reduction of CO_2 capture species on a polycrystalline gold (Au) surface with the selective deposition of each metal CH_4 (g) and CO (f). The kinetics experiments were performed at −1.5 V vs Ag/AgCl for 63 min.

deactivated within the first 7 min corresponding to Ni deposition on the Au active sites. In contrast to CO production, Ni deposited on each of these supports showed similar rates for CH_4 formation. We note that the rate of CH_4 production varies slightly depending on the electrode, where Ni@GC displays a slower rate compared to Ni@Au. Although these differences may be a result of changes in the coverage or dispersion of Ni sites on the various electrodes, we cannot exclude that electronic interactions between the Ni active site and the electrode may also influence the reaction kinetics, although these effects appear to be small. The fact that CH_4 production is observed on each Ni catalyst regardless of the electrode material suggests that Ni is the active species facilitating CH_4 formation and that Au plays no significant role in the reaction. Surprisingly, the reaction rate for CH_4 formation was the smallest for a pure Ni electrode. Using the surface area of the Ni electrode and the rate of CH_4 formation, it is possible to calculate the TOF for pure Ni and compare it to Ni@Au. Details of this calculation can be found in Section S3 of the Supporting Information. These results show that on pure Ni the reaction started with a low turnover frequency of 1.2 mmol (CH_4) mol^{-1} (Ni) s^{-1} and increased to 4.9 mmol (CH_4) mol^{-1} (Ni) s^{-1} by the end of the experiment. This result was the same regardless of addition of EDTA to the electrolyte solution, indicating that Ni alone is responsible for this reaction. These values are much smaller than the TOF of 38 ± 1.6 mmol (CH_4) mol^{-1} (Ni) s^{-1} for Ni@Au, reinforcing the hypothesis that the local structure of Ni atoms plays a more important role than the supporting electrode for this reaction. We also observe that highly dispersed Ni atoms on other surfaces are more active compared to bulk Ni. Although we cannot directly comment on the size distribution of Ni clusters present on the electrode surface, which may be active for CH_4 production, below we describe experimental and theoretical results, which confirm that even single Ni atoms are active for the reduction of carbamate to CH_4, and that this reaction is favored on individually dispersed Ni atoms due to the higher energy required for ammine desorption from bulk Ni.

To better understand the morphology of the active Ni catalyst, we performed the same reaction using Ni deposited on a commercial carbon nanotubes (CNT) electrode. Here Ni was selectively deposited on the CNT using the same protocol

https://doi.org/10.1021/jacs.4c09744
J. Am. Chem. Soc. 2024, 146, 31633−31646

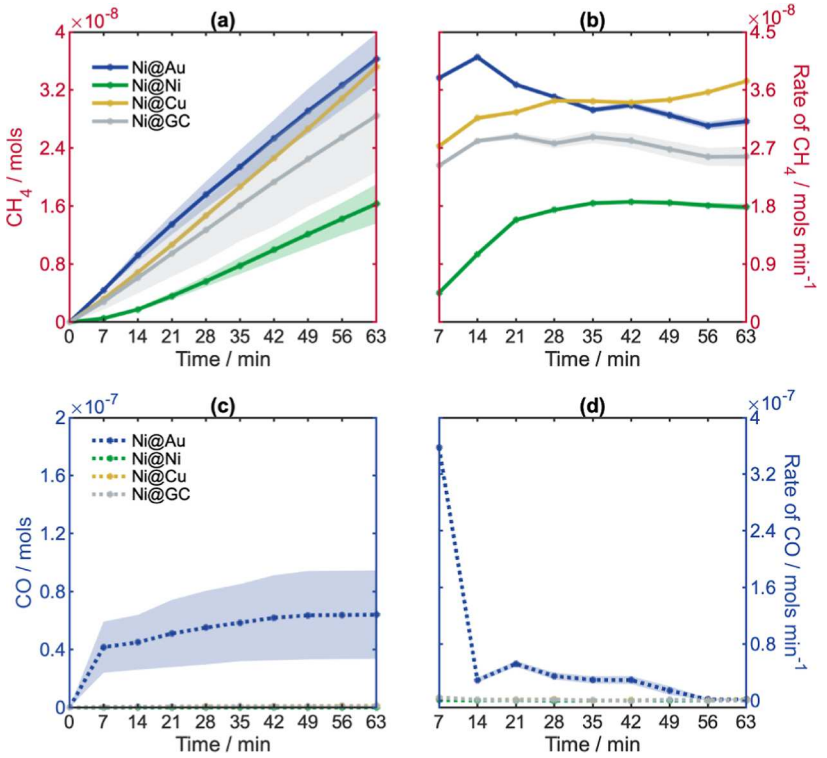

Figure 5. Reduction of CO_2 capture species on different substrates with the selective deposition of trace Ni. Cumulative formation of CH_4 (a) and CO (c) and its respective formation rate (b,d). The kinetics experiments were performed at −1.5 V vs Ag/AgCl for 63 min.

as employed above for the other electrodes. Ni@CNT displayed the highest activity for CH_4 production, as shown in Figure 6a. We note that the CNT electrode has a higher surface area compared to the planar Au, Cu, Ni, and GC electrodes, which results in a higher overall rate of CH_4 production. The corresponding XPS spectra are shown in Figure 6b, which confirm the deposition of Ni on the CNTs following reaction (solid line), while no Ni is detected from the clean CNTs prior to reaction (dashed line). Transmission Electron Microscopy (TEM) and Scanning Transmission Electron Microscopy (STEM) with High-Angle Annular Dark-Field (HAADF) detector were performed of the CNTs before and after the Ni deposition. Figure 6c shows the STEM image of the Ni@CNT catalyst following reaction. For comparison, Figure 6d shows the STEM image of a pristine CNT with no Ni deposited. Although Ni is readily detected in the XPS spectrum of the Ni@CNT sample, we cannot clearly identify the presence of Ni particles in STEM images. Figure S8 of the Supporting Information shows the TEM images and EDX mapping results for the same samples after Ni deposition. None of these images show any indication of Ni particles on the CNTs. We note that some bright spots are detected in the high-angle annular dark-field (HAADF) images with sizes that may correspond to single Ni atoms. However, the EDX signal is below the detection limit for Ni, so it is not possible to confirm the actual identity of these spots. Attempts to obtain atomic resolution of the postdeposition samples is hindered by the presence of the Nafion binding agent that is necessary to prevent dissolution of the CNTs during reaction. The fact that Ni is clearly seen in the XPS, but no Ni particles can be observed by STEM or TEM despite the excellent resolution suggest that Ni is highly dispersed on the CNT electrode, likely as single Ni atoms. Single-atoms are especially challenging to detect by STEM and TEM, and the high energy electron beam can readily eject weakly adsorbed Ni atoms, which are only attached by weak van der Waals forces on the CNT surface.[62,63] However, the detection of bright spots in the STEM-HAADF images, the absence of any observable Ni particles, and the detection of Ni by XPS supports the conclusion that highly dispersed Ni, possibly

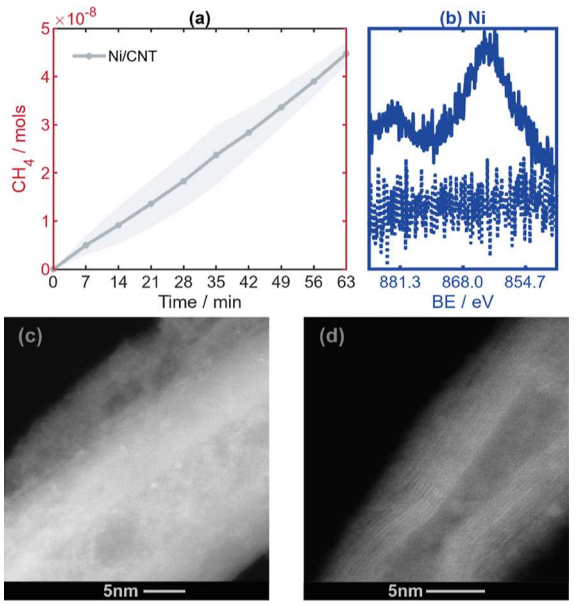

Figure 6. Reduction of CO_2 capture species on Ni/CNT (a). X-ray photoelectron spectra of CNT electrodes before (dashed line) and after (solid line) Ni deposition. (b). Scanning Transmission Electron Microscopy (STEM) with High-Angle Annular Dark-Field (HAADF) image of selective deposited Ni on Carbon Nanotubes (CNT) (c).

https://doi.org/10.1021/jacs.4c09744
J. Am. Chem. Soc. 2024, 146, 31633−31646

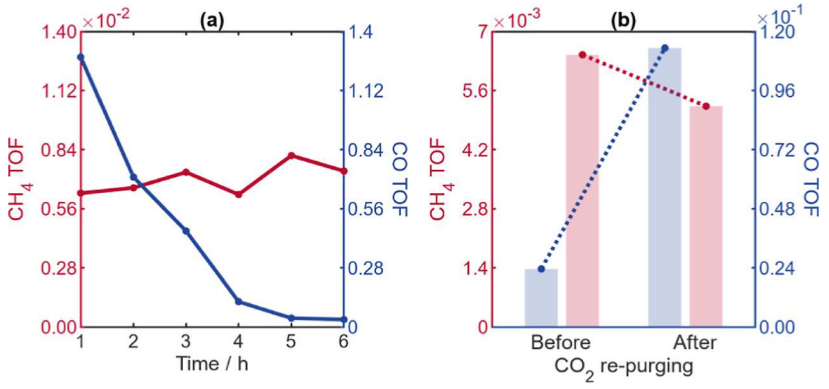

Figure 7. CO TOF and CH_4 TOF for NiPc-OMe/CNT in 1 M MEOA + 0.4 M KCl under −1.5 V vs Ag/AgCl: (a) with continuous N_2 purge during the whole experiment; (b) N_2 purge for the first 3 h, and then purge CO_2 for three mins.

single-atoms, are the catalytic active site responsible for the electrochemical production of CH_4 observed here. This conclusion is further supported by density functional theory (DFT) calculations described below.

To further confirm that single-atom Ni can catalyze carbamate conversion to methane, we conducted additional experiments employing a well-defined single-atom Ni catalyst, i.e. Ni phthalocyanine (NiPc). NiPc is first functionalized with methoxy groups (OMe) to increase the stability, and then molecularly dispersed on carbon nanotubes (CNT) as described previously.[21,64] This NiPc-Ome@CNT catalyst has been shown to show excellent catalytic performance for CO_2 reduction to CO, due to its highly active single-atom Ni sites.[65,66] Additionally, this catalyst remains stable as single-atom molecular catalysts for longer than 40 h under electrochemical reaction conditions making this an excellent system to examine the activity of single-atom Ni for carbamate to CH_4 conversion. In this experiment, the electrolyte is composed of 1 M monoethanolamine (MEOA) with 0.4 M KCl, and it was purged with CO_2 for 1 h, followed by N_2 purge for an additional hour, to fully convert MEA to the capture species while removing dissolved CO_2.

Figure 7a shows that a significant amount of CH_4 is produced from the capture solution employing this NiPc-Ome@CNT catalyst, and the CH_4 TOF remains stable over 6 h. In contrast, although CO has a higher initial TOF than CH_4, the TOF drops quickly, indicating it could be produced from the trace amount of dissolved CO_2 left in the solution after N_2 purge. Although electrochemical kinetics can be influenced by a variety of complex factors, the distinct time-dependent rates of CH_4 and CO formation could be explained by considering that these two products result from reduction of different species, i.e., that that CH_4 is produced from carbamate, which concentration remains stable over the entire reaction, while CO is produced from residual dissolved CO_2, which has a much smaller concentration and is consumed during reaction. Previous studies have shown that it can be difficult to differentiate between reduction of carbamate compared to trace amounts of CO_2. Below we further consider these two possibilities.

In addition to residual CO_2 that is not fully removed from the electrolyte during N_2 purging, free CO_2 may also exist in equilibrium with carbamate. However, this contribution to the total dissolved CO_2 is expected to be small. For example, in the 1 M MEOA electrolyte solution employed here the equilibrium concentration of bulk carbamate is on the order of 30 mM as confirmed by ^{13}C NMR. Given the large equilibrium constant for reaction of CO_2 with MEOA to form carbamate (6.7×10^4),[23] the CO_2 concentration resulting from this equilibrium will be on the order of tens of μM, and this concentration will be even smaller near the interface due to the basic pH gradient. In contrast the solubility of dissolved CO_2 under these conditions is approximately 34 mM. Consequently, if dissolved CO_2 were primarily responsible for CH_4 production, we would expect to observe a significant increase in CH_4 yield upon CO_2 purging, which would increase the concentration of dissolved CO_2 by approximately 3 orders of magnitude.

To evaluate this, we performed another control experiment by introducing CO_2 in the middle of the electrolysis. As shown in Figure 7b, we repeated the exact experiment of Figure 7a but introduced CO_2 by purging the electrolyte for 3 min after 3 h of electrolysis. Figure 7b shows the rates of CO and CH_4 production immediately before and after CO_2 purging. Interestingly, the CO TOF increases by *a* factor of 5 immediately after CO_2 purging while CH_4 TOF does not change. This fact can be rationalized by assuming that CO is produced from dissolved CO_2, whose concentration recovers after introducing external CO_2, while CH_4 is produced primarily from carbamate, whose concentration would not change when adding a small amount of external CO_2. While we cannot fully exclude the possibility that dissolved CO_2 may also be reduced to CH_4 by Ni, we find that this contribution is minor compared to direct carbamate reduction. This can be further seen in Figure S9, when using 1 M TEA + 0.4 M KCl as the electrolyte, where no carbamate can form in the capture solution due to the tertiary amine, similar to Figure 1c. As shown, in the TEA capture solution both CO and CH_4 formation were detected; however, the TOF for CH_4 was *a* factor of 10 lower than observed in MEOA. Additionally, we observed that both CO and CH_4 production rates decrease quickly over time, corresponding to the consumption of dissolved CO_2 unlike in MEOA where the CH_4 production rate is constant for more than 6 h. Together these results confirm that dissolved CO_2 represents only a minor contribution to CH_4 formation, while the source for CO formation is due almost entirely to dissolved CO_2. In summary, these findings show that single-atom Ni catalysts, including NiPc-OMe/CNT as well as highly dispersed Ni electrodeposited on any conductive electrode surface, are capable of the direct conversion of carbamate to CH_4. To better

https://doi.org/10.1021/jacs.4c09744
J. Am. Chem. Soc. 2024, 146, 31633−31646

understand the mechanism for this reaction, we turn to DFT calculations.

DFT calculations were used to model the mechanism of carbamate reduction on dispersed Ni atoms on Au electrodes. We chose to model Ni dispersed on Au because it is known that pure Au electrodes produce only CO in aqueous CO_2 electroreduction.[67−69] We employed a Au(211) step as a model for the electrode surface, where a single Ni atom is substituted for one of the Au atoms on the step to represent the dispersed Ni atoms. This surface model is denoted Ni@Au(211). The (211) step was used for mechanistic studies because Ni most likely deposits near the uncoordinated surface atoms on the step; such stepped surface models are also commonly employed in other first-principles studies of CO_2 electroreduction catalysis.[70−73] The Ni dispersion on the Ni@Au(211) model is 8.3% of the monolayer, which is approximately equal to the experimental value measured by XPS, as shown in Table 1. We assume that carbamate is eventually adsorbed to Ni@Au(211) as neutral carbamic acid, either through outer-sphere proton transfer or inner-sphere proton-coupled electron transfer (PCET) while adsorbed to the catalyst surface. Thus, various binding configurations of carbamic acid to Ni@Au(211) were considered, where different atoms in carbamic acid can bind to different adsorption sites. The most stable binding configuration of carbamic acid is shown in Figure 8 as H_2NCOOH^*, where * denotes that the species is adsorbed on the surface. This specie is also marked with a red border in Figure S10. We found that H_2NCOOH^* binds through oxygen to the Ni top site. Additional optimized H_2NCOOH^* structures considered are shown in Figure S10.

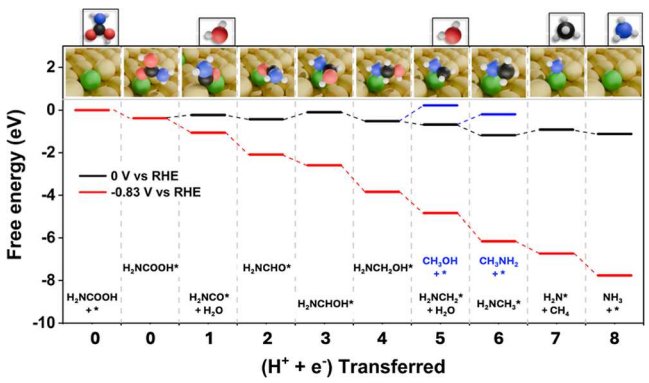

Figure 8. Calculated free energy diagram on Ni@Au(211). The black pathway represents carbamic acid reduction at 0 V vs RHE and the red pathway represents the reaction pathway at −0.83 V vs RHE. The two separate blue lines show alternate, higher energy pathways for the formation of methanol and methylamine at 0 V vs RHE. Note that * denotes either a surface site or an adsorbed species on the surface. Here, gold is represented in yellow, nickel in green, hydrogen in white, oxygen in red, carbon in black, and nitrogen in blue.

Following the adsorption of carbamic acid to Ni@Au(211), H_2NCOOH^* can subsequently be reduced through multiple PCET reactions at the reducing potentials required for CO_2 electroreduction. Because of the molecular heterogeneity of H_2NCOOH^* as well as the other adsorbed reaction intermediates, these PCET reactions can involve protonation of either N, C, or O atoms of the adsorbate. Moreover, adsorption may involve different atoms of the adsorbate coordinated to the surface or alternate geometric configurations resulting from the successive protonation. Though many configurations of the intermediates were considered, as shown in Figure S10, only the most thermodynamically favorable pathways are shown in Figure 8 for clarity.

Figure 8 shows the free energy diagram and intermediate geometries for carbamate reduction on Ni@Au(211). We used the computational hydrogen electrode (CHE) model to calculate the potential-dependent free energies of reaction intermediates. Although applied potential effects are simplified within the CHE model compared to other approaches such as grand-canonical DFT,[74−80] we note that simplified models using the CHE method can still be used to explore plausible reaction mechanisms and elucidate reactivity trends as shown in previous work.[70,81−84] The calculated work functions of the intermediates in Figure 8 suggest modest capacitive contributions to the reaction free energies (Table S2).[85] Using the computational hydrogen electrode (CHE) model,[86] the reaction pathways are calculated at 0 and −0.83 V vs RHE (shown in black and red, respectively). There are three general possibilities for the first PCET reaction to adsorbed carbamic acid, $H_2NCHOOH^*$: protonation of the O atom to produce H_2NCO^* and liberate an H_2O molecule, protonation of the N atom to produce $COOH^*$ and liberate an NH_3 molecule, or protonation of the C atom to produce $H_2NCHOOH^*$. Among these possibilities, the protonation of the O atom to form H_2NCO^* and H_2O is the most thermodynamically favorable at 0 V (ΔG = 0.16 eV), compared to protonation of the N atom (ΔG = 0.93 eV) or the C atom (ΔG = 0.56 eV). This intermediate, formed after the first PCET step, is shown in Figure 8. Following this general procedure, the subsequent PCET steps were analyzed accordingly. We also considered the dissociation of the N−C bond in H_2NCO^* to form CO and NH_2^*. This process has a ΔG of 1.45 eV, whereas PCET to form H_2NCHO^* is more thermodynamically favorable with a ΔG of −0.20 eV at 0 V vs RHE. This suggests that CO formation is thermodynamically unfavorable on Ni@Au catalysts, in agreement with the experimental results. Initially, the reaction intermediates are bound to Ni through oxygen. In the third PCET step to form the intermediate H_2NCHOH^*, however, the most stable adsorbate configuration involves binding to Ni through nitrogen. The calculations show that subsequent intermediates in the most thermodynamically favorable reaction pathway also bind to Ni through N. The binding of H_2NCHOH^* through nitrogen is critical for the selective conversion of carbamate to CH_4 because the O and C atoms are more accessible to transferring protons in this binding configuration. In the fifth PCET step, for example, the O atom is protonated, releasing H_2O and leaving $H_2NCH_2^*$ on the surface. In the seventh PCET step, the C atom of $H_2NCH_3^*$ is protonated, releasing the CH_4 product and leaving NH_2^* on the surface. A subsequent PCET to NH_2^* produces NH_3, regenerates the active site, and closes the catalytic cycle. The detailed geometric structures are presented in Figure S10 and the free energies of the optimized adsorbed species are presented in Table S2. The standard reaction free energies at 0 V vs RHE corresponding to the elementary steps shown in Figure 8 are tabulated in Table S1. The red pathway in Figure 8 represents the free energy diagram at −0.83 V vs RHE, which is equivalent to −1.5 V vs Ag/AgCl at pH 8. It is observed that at this potential all the reaction steps are exergonic and able to produce CH_4 successfully from carbamate.

https://doi.org/10.1021/jacs.4c09744
J. Am. Chem. Soc. 2024, 146, 31633−31646

Given the various potential protonation sites of the adsorbates involved in the reaction, alternate reaction pathways were also considered. Other possible reaction intermediates are shown in Figure S10. A subset of these alternate reaction mechanisms is shown in Figure 8, where the pathway at 0 V vs RHE includes two alternate reaction steps marked by blue lines. Rather than releasing H_2O and forming H_2NCH_2* in the fifth PCET step, there is a possibility to form CH_3OH by protonating the carbon of H_2NCH_2OH*. However, the free energy diagram at 0 V vs RHE in Figure 8 shows that O protonation is thermodynamically favored over C protonation to form CH_3OH. This result indicates that CH_3OH formation is thermodynamically unfavorable. These computational predictions align with the absence of CH_3OH in the NMR spectroscopy results. Similarly, there is the possibility of methylamine (CH_3NH_2) desorption in the sixth PCET step; however, this desorption is endothermic and thus CH_3NH_2* remains chemisorbed on the surface. Overall, the thermodynamic analyses suggest that CH_4 should be the dominant product formed for dispersed Ni sites on Au electrodes.

To evaluate whether C−N bond cleavage is the final step in the formation of CH_4 from carbamate as predicted by DFT, we performed electrochemical kinetics for CO and HCOOH reduction. These two intermediates could be formed as alternative branching pathways during either the first or second proton/electron transfer steps shown in Figure 6 and subsequently reduced to CH_4. For CO reduction measurements, the same NH_3 + KOH electrolyte solution was purged with pure CO at 1 atm, and a pure CO atmosphere was kept as the cell headspace, which was continuously recirculated inside the solution. For HCOOH reduction measurements, 5 mM concentration of HCOOH was added to this electrolyte followed by N_2 purging. In both cases, we observed no detectable CH_4 during 1 h of electrolysis. These results are consistent with DFT calculations, which show that for carbamate reduction on Ni single atoms, cleavage of the C−N bond is the final step prior to production of CH_4 and recovery of the amine.

To compare the results for dispersed Ni atom reactivity to bulk Ni, Figure 9 shows the free energy diagram for the carbamate reduction mechanism on Ni(211). A similar procedure was used to analyze the mechanism on a clean Ni(211) surface, as was done for Ni@Au(211) in Figure 8. The free energy diagrams at −0.83 V vs RHE for Ni(211) and Ni@Au(211) (red) are represented in Figure 9 in black and red, respectively. Note that −0.83 V vs RHE is calculated to be the thermodynamic limiting potential for carbamate reduction on Ni@Au(211) as shown in Figure 8. The calculations demonstrate that carbamic acid adsorption on Ni(211) is 0.16 eV less exothermic than Ni@Au(211). Moreover, the final step of the reaction on Ni(211) is uphill at −0.83 V vs RHE, meaning that a larger overpotential is needed to produce NH_3 and close the catalytic cycle. The computational results demonstrate a feasible route to CH_4 from carbamate on Ni@Au(211) and provide thermodynamic evidence for the enhanced reactivity over bulk Ni electrodes. These trends are in agreement with experimental rate measurements in Figure 5. Future modeling studies are needed to further elucidate the effects of surface charge and solvation on the kinetics of carbamate reduction, which can aid in the development of electrocatalytic systems to selectively convert CO_2 capture solutions to desired products.

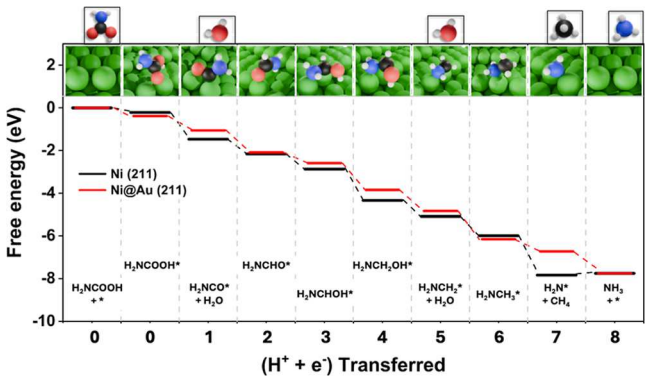

Figure 9. Comparison of calculated free energy diagram on Ni(211) and Ni@Au(211). The black pathway represents carbamic acid reduction on Ni(211) at −0.83 V vs RHE and the red pathway represents the reaction pathway on Ni@Au(211) at −0.83 V vs RHE. Note that * denotes either a surface site or an adsorbed species on the surface. Here, nickel is represented in green, hydrogen in white, oxygen in red, carbon in black, and nitrogen in blue.

CONCLUSIONS

This study describes for the first time the electrochemical conversion of carbamate species to CH_4. A detailed study employing XPS, STEM and control experiments involving molecularly defined single-atom NiPc dispersed on CNT (NiPc-OMe@CNT) demonstrate that atomically dispersed Ni catalyst on various surfaces is uniquely active for this reaction, making this catalyst highly selective to CH_4 over other C-based products. The mechanism of this process is understood with the aid of DFT calculations, which confirm that the conversion of carbamate to CH_4 on Ni single-atoms deposited on Au (Ni@Au) is favored over other possible products, including CO, methylated amine and methanol. The calculations also demonstrate that while the reaction may proceed even on bulk Ni, it is kinetically favored on single Ni atoms due to the kinetic barrier associated with desorption of the regenerated amine on bulk Ni. Overall, this study identifies a new class of catalysts capable of directly converting carbamate to CH_4 and provides key mechanistic insight into guide future applications based on the electrochemical conversion of CO_2 capture species directly to hydrocarbon products.

ASSOCIATED CONTENT

Supporting Information

The Supporting Information is available free of charge at https://pubs.acs.org/doi/10.1021/jacs.4c09744.

Methods; H_2 evolution and CO kinetics; XPS survey spectra and coverage calculations; Capture Solution and Ni/Au Stability; TEM and EDX imaging, Ni phthalocyanine control experiments, additional DFT calculations (PDF)

AUTHOR INFORMATION

Corresponding Authors

Hailiang Wang − *Department of Chemistry, Yale University, New Haven, Connecticut 06520, United States; Energy Sciences Institute, Yale University, West Haven, Connecticut 06516, United States;* orcid.org/0000-0003-4409-2034; Email: hailiang.wang@yale.edu

Liane M. Rossi − *Departamento de Química Fundamental, Instituto de Química, Universidade de São Paulo, São Paulo, São Paulo 05508-000, Brazil;* orcid.org/0000-0001-7679-0852; Email: lrossi@iq.usp.br

Robert E. Warburton − *Case Western Reserve University, Cleveland, Ohio 44106, United States;* orcid.org/0000-0002-9693-307X; Email: rew134@case.edu

L. Robert Baker − *Department of Chemistry and Biochemistry, The Ohio State University, Columbus, Ohio 43210, United States;* orcid.org/0000-0001-6740-864X; Email: baker.2364@osu.edu

Authors

Tomaz Neves-Garcia − *Department of Chemistry and Biochemistry, The Ohio State University, Columbus, Ohio 43210, United States; Departamento de Química Fundamental, Instituto de Química, Universidade de São Paulo, São Paulo, São Paulo 05508-000, Brazil;* orcid.org/0000-0002-7220-9423

Mahmudul Hasan − *Case Western Reserve University, Cleveland, Ohio 44106, United States*

Quansong Zhu − *Department of Chemistry and Biochemistry, The Ohio State University, Columbus, Ohio 43210, United States;* orcid.org/0000-0002-5376-1247

Jing Li − *Department of Chemistry, Yale University, New Haven, Connecticut 06520, United States; Energy Sciences Institute, Yale University, West Haven, Connecticut 06516, United States;* orcid.org/0000-0001-7538-246X

Zhan Jiang − *Shenzhen Key Laboratory of Printed Electronics, Southern University of Science and Technology, Shenzhen 518055, P. R. China; Department of Materials Science and Engineering, Southern University of Science and Technology, Shenzhen 518055, P. R. China*

Yongye Liang − *Shenzhen Key Laboratory of Printed Electronics, Southern University of Science and Technology, Shenzhen 518055, P. R. China; Department of Materials Science and Engineering, Southern University of Science and Technology, Shenzhen 518055, P. R. China;* orcid.org/0000-0002-7416-8792

Complete contact information is available at: https://pubs.acs.org/10.1021/jacs.4c09744

Notes

The authors declare no competing financial interest.

■ ACKNOWLEDGMENTS

Electrocatalysis measurements and catalyst characterization was supported by the Catalysis Science Program in the Chemical Science Geosciences and Biosciences Division of the Office of Basic Energy Sciences of the U.S. Department of Energy under grant number DE-SC0024157. Preparation of the NiPc-OMe catalyst was supported by the U.S. National Science Foundation under grant number CHE-2154724. R.E.W. acknowledges start-up funding support from the Case School of Engineering. This work made use of the High Performance Computing Resource in the Core Facility for Advanced Research Computing at Case Western Reserve University and the Ohio Supercomputer Center.[87] This research also used resources of the National Energy Research Scientific Computing Center, a DOE Office of Science User Facility supported by the Office of Science of the U.S. Department of Energy under Contract no. DE-AC02-05CH11231. T.N.G. would like to thank Fundação de Amparo à Pesquisa do Estado de São Paulo (FAPESP) for individual funding under award number 2017/24347−0. Thin film deposition was performed at the NanoSystems Laboratory at The Ohio State University, which is supported by the Center for Emergent Materials: an NSF MRSEC under award number DMR-2011876. Electron microscopy was performed at the Center for Electron Microscopy and Analysis at The Ohio State University. XPS measurements were performed at the Surface Analysis Laboratory at The Ohio State University. The authors thank Dr. Robert Williams for assistance with electron microscopy, Dr. Yehia Khalifa for assistance with XPS measurements and analysis, and Noah South for helpful discussions.

■ ABBREVIATIONS

CO_2, carbon dioxide; CO, carbon monoxide; CH_4, methane; N_2, nitrogen; Au, gold; Ag, silver; Cu, cupper; Ni, nickel; Fe, iron; Zn, zinc; Pb, lead; Ni-Pc, nickel phthalocyanine; CNT, carbon nanotubes; NH_3, ammonia; EDA, ethylenediamine; MEOA, monoethanolamine; MEA, monoethylamine; DEA, diethylamine; TEA, triethylamine; KOH, potassium hydroxide; EDTA, ethylenediaminetetraacetic acid; HER, hydrogen evolution reaction; EDL, electrical doble layer; Ag/AgCl, silver/silver chloride reference electrode; DFT, density functional theory; NMR, nuclear magnetic resonance; XPS, X-ray photoelectron spectroscopy

■ REFERENCES

(1) Shukla, P. R.; Skea, J.; Slade, R.; Al Khourdajie, A.; van Diemen, R.; McCollum, D.; Pathak, M.; Some, S.; Vyas, P.; Fradera, R.; et al. *Climate Change 2022: Mitigation of Climate Change*. Contribution of Working Group III to the Sixth Assessment Report of the Intergovernmental Panel on Climate Change; Cambridge University Press, 2022..

(2) Mac Dowell, N.; Fennell, P. S.; Shah, N.; Maitland, G. C. The role of CO_2 capture and utilization in mitigating climate change. *Nat. Clim. Change* **2017**, *7* (4), 243−249.

(3) Fiorio, J. L.; Borges, L. R.; Neves-Garcia, T.; Kikuchi, D. K.; Guerra, R. R. G.; Rossi, L. M. Design of gold catalysts for activation of H_2 and H-donor molecules: transfer hydrogenation and CO_2 hydrogenation. *Catal. Sci. Technol.* **2023**, *13* (11), 3205−3215.

(4) Liang, Z.; Rongwong, W.; Liu, H.; Fu, K.; Gao, H.; Cao, F.; Zhang, R.; Sema, T.; Henni, A.; Sumon, K.; et al. Recent progress and new developments in post-combustion carbon-capture technology with amine based solvents. *Int. J. Greenhouse Gas Control* **2015**, *40*, 26−54.

(5) Dutcher, B.; Fan, M.; Russell, A. G. Amine-Based CO_2 Capture Technology Development from the Beginning of 2013—A Review. *ACS Appl. Mater. Interfaces* **2015**, *7* (4), 2137−2148.

(6) Rainbolt, J. E.; Koech, P. K.; Yonker, C. R.; Zheng, F.; Main, D.; Weaver, M. L.; Linehan, J. C.; Heldebrant, D. J. Anhydrous tertiary alkanolamines as hybrid chemical and physical CO_2 capture reagents with pressure-swing regeneration. *Energy Environ. Sci.* **2011**, *4* (2), 480−484.

(7) Bui, M.; Adjiman, C. S.; Bardow, A.; Anthony, E. J.; Boston, A.; Brown, S.; Fennell, P. S.; Fuss, S.; Galindo, A.; Hackett, L. A.; et al. Carbon capture and storage (CCS): the way forward. *Energy Environ. Sci.* **2018**, *11* (5), 1062−1176.

(8) Rochelle, G. T. Amine Scrubbing for CO_2 Capture. *Science* **2009**, *325* (5948), 1652−1654.

(9) Liu, Q.; Wu, L.; Jackstell, R.; Beller, M. Using carbon dioxide as a building block in organic synthesis. *Nat. Commun.* **2015**, *6* (1), 5933.

(10) Langie, K.; Bak, G.; Lee, U.; Lee, D. K.; Lee, C. W.; Hwang, Y. J.; Won, D. H. Advances in the direct electro-conversion of captured

CO_2 into valuable products. *J. Mater. Chem. A* **2024**, *12* (18), 10597−10613.
(11) Sullivan, I.; Goryachev, A.; Digdaya, I. A.; Li, X.; Atwater, H. A.; Vermaas, D. A.; Xiang, C. Coupling electrochemical CO_2 conversion with CO_2 capture. *Nat. Catal.* **2021**, *4* (11), 952−958.
(12) Kim, S.; Shin, H.; Kang, J. S. Electrochemical reduction of captured CO_2: A route toward the integrated carbon capture and utilization. *Curr. Opin. Electrochem.* **2023**, *40*, 101321.
(13) Jerng, S. E.; Gallant, B. M. Electrochemical reduction of CO_2 in the captured state using aqueous or nonaqueous amines. *iScience* **2022**, *25* (7), 104558.
(14) Li, M.; Irtem, E.; Iglesias Van Montfort, H.-P.; Abdinejad, M.; Burdyny, T. Energy comparison of sequential and integrated CO_2 capture and electrochemical conversion. *Nat. Commun.* **2022**, *13* (1), 5398.
(15) Kumar De, S.; Won, D.-I.; Kim, J.; Kim, D. H. Integrated CO_2capture and electrochemical upgradation: the underpinning mechanism and techno-chemical analysis. *Chem. Soc. Rev.* **2023**, *52* (16), 5744−5802.
(16) Xia, Q.; Zhang, K.; Zheng, T.; An, L.; Xia, C.; Zhang, X. Integration of CO_2 Capture and Electrochemical Conversion. *ACS Energy Lett.* **2023**, *8* (6), 2840−2857.
(17) Zhang, W.; Yang, Y.; Li, Y.; Li, F.; Luo, M. Recent progress on integrated CO_2 capture and electrochemical upgrading. *Mater. Today. Catal.* **2023**, *2*, 100006.
(18) Zhang, K.; Guo, D.; Wang, X.; Qin, Y.; Hu, L.; Zhang, Y.; Zou, R.; Gao, S. Sustainable CO_2 management through integrated CO_2 capture and conversion. *J. CO_2 Util.* **2023**, *72*, 102493.
(19) Lee, S.; Choi, W.; Kim, J. H.; Park, S.; Hwang, Y. J.; Na, J. Techno-economic analysis and life-cycle assessment of the electrochemical conversion process with captured CO_2 in an amine-based solvent. *Green Chem.* **2023**, *25* (24), 10398−10414.
(20) Chen, L.; Li, F.; Zhang, Y.; Bentley, C. L.; Horne, M.; Bond, A. M.; Zhang, J. Electrochemical Reduction of Carbon Dioxide in a Monoethanolamine Capture Medium. *ChemSusChem* **2017**, *10* (20), 4109−4118.
(21) Kim, J. H.; Jang, H.; Bak, G.; Choi, W.; Yun, H.; Lee, E.; Kim, D.; Kim, J.; Lee, S. Y.; Hwang, Y. J. The insensitive cation effect on a single-atom Ni catalyst allows selective electrochemical conversion of captured CO_2 in universal media. *Energy Environ. Sci.* **2022**, *15* (10), 4301−4312.
(22) Hossain, M. N.; Ahmad, S.; Da Silva, I. S.; Kraatz, H. B. Electrochemical Reduction of CO_2 at Coinage Metal Nanodendrites in Aqueous Ethanolamine. *Chem.—Eur. J.* **2021**, *27* (4), 1346−1355.
(23) Safipour, J.; Weber, A. Z.; Bell, A. T. Detrimental Effects of Monoethanolamine and Other Amine-Based Capture Agents on the Electrochemical Reduction of CO_2. *ACS Energy Lett.* **2023**, *8* (12), 5012−5017.
(24) Deng, G.-H.; Zhu, Q.; Rebstock, J.; Neves-Garcia, T.; Baker, L. R. Direct observation of bicarbonate and water reduction on gold: understanding the potential dependent proton source during hydrogen evolution. *Chem. Sci.* **2023**, *14* (17), 4523−4531.
(25) Choi, J.; Chiu, S.; Banerjee, A.; Sacci, R. L.; Veith, G. M.; Stieber, C.; Hahn, C.; Alexandrova, A. N.; Morales-Guio, C. G. Corrosion and Enhanced Hydrogen Evolution in Electrochemical Reduction of Ammonium Carbamate on Transition Metal Surfaces. *ChemRxiv* **2024**.
(26) Shen, K.; Cheng, D.; Reyes-Lopez, E.; Jang, J.; Sautet, P.; Morales-Guio, C. G. On the origin of carbon sources in the electrochemical upgrade of CO_2 from carbon capture solutions. *Joule* **2023**, *7* (6), 1260−1276.
(27) Leverick, G.; Bernhardt, E. M.; Ismail, A. I.; Law, J. H.; Arifutzzaman, A.; Aroua, M. K.; Gallant, B. M. Uncovering the Active Species in Amine-Mediated CO_2 Reduction to CO on Ag. *ACS Catal.* **2023**, *13* (18), 12322−12337.
(28) Creţu, R.; Kellenberger, A.; Vaszilcsin, N. Enhancement of hydrogen evolution reaction on platinum cathode by proton carriers. *Int. J. Hydrogen Energy* **2013**, *38* (27), 11685.
(29) Gutiérrez-Sánchez, O.; Bohlen, B.; Daems, N.; Bulut, M.; Pant, D.; Breugelmans, T. A. State-of-the-Art Update on Integrated CO_2 Capture and Electrochemical Conversion Systems. *ChemElectroChem* **2022**, *9* (5), No. e202101540.
(30) Abdinejad, M.; Mirza, Z.; Zhang, X.-A.; Kraatz, H.-B. Enhanced Electrocatalytic Activity of Primary Amines for CO_2 Reduction Using Copper Electrodes in Aqueous Solution. *ACS Sustainable Chem. Eng.* **2020**, *8* (4), 1715−1720.
(31) Lee, G.; Li, Y. C.; Kim, J.-Y.; Peng, T.; Nam, D.-H.; Sedighian Rasouli, A.; Li, F.; Luo, M.; Ip, A. H.; Joo, Y.-C.; Sargent, E.-H.; et al. Electrochemical upgrade of CO_2 from amine capture solution. *Nat. Energy* **2021**, *6* (1), 46.
(32) Liu, M.; Zhan, L.; Wang, Y.; Zhao, X.; Wu, J.; Deng, D.; Jiang, J.; Zheng, X.; Lei, Y. Achieving integrated capture and reduction of CO_2: A promising electrocatalyst. *J. Mater. Sci. Technol.* **2023**, *165*, 235−243.
(33) Bhattacharya, M.; Sebghati, S.; VanderLinden, R. T.; Saouma, C. T. Toward Combined Carbon Capture and Recycling: Addition of an Amine Alters Product Selectivity from CO to Formic Acid in Manganese Catalyzed Reduction of CO_2. *J. Am. Chem. Soc.* **2020**, *142* (41), 17589−17597.
(34) Jilvero, H.; Normann, F.; Andersson, K.; Johnsson, F. The Rate of CO_2 Absorption in Ammonia—Implications on Absorber Design. *Ind. Eng. Chem. Res.* **2014**, *53* (16), 6750−6758.
(35) Liu, H.; Chen, Y.; Lee, J.; Gu, S.; Li, W. Ammonia-Mediated CO_2 Capture and Direct Electroreduction to Formate. *ACS Energy Lett.* **2022**, *7* (12), 4483−4489.
(36) Bhattacharya, M.; Sebghati, S.; Vercella, Y. M.; Saouma, C. T. Electrochemical Reduction of Carbamates and Carbamic Acids: Implications for Combined Carbon Capture and Electrochemical CO_2 Recycling. *J. Electrochem. Soc.* **2020**, *167* (8), 086507.
(37) Li, T.; Shao, M. A minireview on electrochemical CO_2 conversion based on carbonate/bicarbonate media. *EES Catalysis* **2024**, *2* (2), 564−572.
(38) Khurram, A.; Yan, L.; Yin, Y.; Zhao, L.; Gallant, B. M. Promoting Amine-Activated Electrochemical CO_2 Conversion with Alkali Salts. *J. Phys. Chem. C* **2019**, *123* (30), 18222−18231.
(39) Ahn, C. K.; Lee, H. W.; Lee, M. W.; Chang, Y. S.; Han, K.; Rhee, C. H.; Kim, J. Y.; Chun, H. D.; Park, J. M. Determination of ammonium salt/ion speciation in the CO_2 absorption process using ammonia solution: Modeling and experimental approaches. *Energy Procedia* **2011**, *4*, 541−547.
(40) Kortunov, P. V.; Siskin, M.; Baugh, L. S.; Calabro, D. C. In Situ Nuclear Magnetic Resonance Mechanistic Studies of Carbon Dioxide Reactions with Liquid Amines in Aqueous Systems: New Insights on Carbon Capture Reaction Pathways. *Energy Fuels* **2015**, *29* (9), 5919−5939.
(41) Wang, X.; Conway, W.; Fernandes, D.; Lawrance, G.; Burns, R.; Puxty, G.; Maeder, M. Kinetics of the Reversible Reaction of CO_2(aq) with Ammonia in Aqueous Solution. *J. Phys. Chem. A* **2011**, *115* (24), 6405−6412.
(42) Mani, F.; Peruzzini, M.; Stoppioni, P. CO_2 absorption by aqueous NH_3 solutions: speciation of ammonium carbamate, bicarbonate and carbonate by a ^{13}C NMR study. *Green Chem.* **2006**, *8* (11), 995.
(43) Park, H.; Jung, Y. M.; You, J. K.; Hong, W. H.; Kim, J.-N. Analysis of the CO_2 and NH_3 Reaction in an Aqueous Solution by 2D IR COS: Formation of Bicarbonate and Carbamate. *J. Phys. Chem. A* **2008**, *112* (29), 6558−6562.
(44) Yang, X.; Rees, R. J.; Conway, W.; Puxty, G.; Yang, Q.; Winkler, D. A. Computational Modeling and Simulation of CO_2 Capture by Aqueous Amines. *Chem. Rev.* **2017**, *117* (14), 9524−9593.
(45) Holmes, P. E.; Naaz, M.; Poling, B. E. Ion Concentrations in the CO_2−NH_3−H_2O System from ^{13}C NMR Spectroscopy. *Ind. Eng. Chem. Res.* **1998**, *37* (8), 3281−3287.
(46) Yamada, H. Amine-based capture of CO2 for utilization and storage. *Polym. J.* **2021**, *53* (1), 93−102.

(47) Kim, Y. J.; You, J. K.; Hong, W. H.; Yi, K. B.; Ko, C. H.; Kim, J. N. Characteristics of CO_2 Absorption into Aqueous Ammonia. *Sep. Sci. Technol.* **2008**, *43* (4), 766−777.
(48) Ahn, C. K.; Lee, H. W.; Chang, Y. S.; Han, K.; Kim, J. Y.; Rhee, C. H.; Chun, H. D.; Lee, M. W.; Park, J. M. Characterization of ammonia-based CO_2 capture process using ion speciation. *Int. J. Greenhouse Gas Control* **2011**, *5* (6), 1606−1613.
(49) Kim, D. Y.; Lee, H. M.; Min, S. K.; Cho, Y.; Hwang, I.-C.; Han, K.; Kim, J. Y.; Kim, K. S. CO_2 Capturing Mechanism in Aqueous Ammonia: NH_3-Driven Decomposition−Recombination Pathway. *J. Phys. Chem. Lett.* **2011**, *2* (7), 689−694.
(50) Meng, F.; Meng, Y.; Ju, T.; Han, S.; Lin, L.; Jiang, J. Research progress of aqueous amine solution for CO2 capture: A review. *Renewable Sustainable Energy Rev.* **2022**, *168*, 112902.
(51) Deng, B.; Huang, M.; Zhao, X.; Mou, S.; Dong, F. Interfacial Electrolyte Effects on Electrocatalytic CO_2 Reduction. *ACS Catal.* **2022**, *12* (1), 331−362.
(52) Kas, R.; Kortlever, R.; Yılmaz, H.; Koper, M. T. M.; Mul, G. Manipulating the Hydrocarbon Selectivity of Copper Nanoparticles in CO_2 Electroreduction by Process Conditions. *ChemElectroChem* **2015**, *2* (3), 354−358.
(53) Carneiro-Neto, E. B.; Lopes, M. C.; Pereira, E. C. Simulation of interfacial pH changes during hydrogen evolution reaction. *J. Electroanal. Chem.* **2016**, *765*, 92−99.
(54) Rebstock, J. A.; Zhu, Q.; Baker, L. R. Comparing interfacial cation hydration at catalytic active sites and spectator sites on gold electrodes: understanding structure sensitive CO_2 reduction kinetics. *Chem. Sci.* **2022**, *13* (25), 7634−7643.
(55) Wuttig, A.; Surendranath, Y. Impurity Ion Complexation Enhances Carbon Dioxide Reduction Catalysis. *ACS Catal.* **2015**, *5* (7), 4479−4484.
(56) Hori, Y.; Konishi, H.; Futamura, T.; Murata, A.; Koga, O.; Sakurai, H.; Oguma, K. Deactivation of copper electrode" in electrochemical reduction of CO_2. *Electrochim. Acta* **2005**, *50* (27), 5354−5369.
(57) Hori, Y.. In *Electrochemical CO2 Reduction on Metal Electrodes. In Modern Aspects of Electrochemistry*; Vayenas, C. G., White, R. E., Gamboa-Aldeco, M. E., Eds.; Springer: New York, 2008; pp 89−189.
(58) Cui, Z.; Marx, M. A.; Tegomoh, M. N.; Co, A. C. A Guide to Evaluate Electrolyte Purity for CO_2 Reduction Studies. *ACS Energy Lett.* **2023**, *8* (12), 5201−5205.
(59) He, J.; Huang, A.; Johnson, N. J. J.; Dettelbach, K. E.; Weekes, D. M.; Cao, Y.; Berlinguette, C. P. Stabilizing Copper for CO_2 Reduction in Low-Grade Electrolyte. *Inorg. Chem.* **2018**, *57* (23), 14624−14631.
(60) Shang, H.; Wallentine, S. K.; Hofmann, D. M.; Zhu, Q.; Murphy, C. J.; Baker, L. R. Effect of surface ligands on gold nanocatalysts for CO_2 reduction. *Chem. Sci.* **2020**, *11* (45), 12298−12306.
(61) Weber, D. J.; Dosche, C.; Oezaslan, M. Fundamental Aspects of Contamination during the Hydrogen Evolution/Oxidation Reaction in Alkaline Media. *J. Electrochem. Soc.* **2020**, *167* (2), 024506.
(62) Egerton, R. F.; Li, P.; Malac, M. Radiation damage in the TEM and SEM. *Micron* **2004**, *35* (6), 399−409.
(63) Jain, M.; Kretschmer, S.; Meyer, J.; Krasheninnikov, A. V. Adatom-mediated damage of two-dimensional materials under the electron beam in a transmission electron microscope. *Phys. Rev. Mater.* **2024**, *8* (5), 054004.
(64) Zhou, Y.; Zhou, Q.; Liu, H.; Xu, W.; Wang, Z.; Qiao, S.; Ding, H.; Chen, D.; Zhu, J.; Qi, Z.; et al. Asymmetric dinitrogen-coordinated nickel single-atomic sites for efficient CO_2 electroreduction. *Nat. Commun.* **2023**, *14* (1), 3776.
(65) Zhang, X.; Wang, Y.; Gu, M.; Wang, M.; Zhang, Z.; Pan, W.; Jiang, Z.; Zheng, H.; Lucero, M.; Wang, H.; et al. Molecular engineering of dispersed nickel phthalocyanines on carbon nanotubes for selective CO_2 reduction. *Nat. Energy* **2020**, *5* (9), 684−692.
(66) Jiang, Z.; Zhang, Z.; Li, H.; Tang, Y.; Yuan, Y.; Zao, J.; Zheng, H.; Liang, Y. Molecular Catalyst with Near 100% Selectivity for CO_2 Reduction in Acidic Electrolytes. *Adv. Energy Mater.* **2023**, *13* (6), 2203603.
(67) Goyal, A.; Marcandalli, G.; Mints, V. A.; Koper, M. T. M. Competition between CO_2 Reduction and Hydrogen Evolution on a Gold Electrode under Well-Defined Mass Transport Conditions. *J. Am. Chem. Soc.* **2020**, *142* (9), 4154−4161.
(68) Hall, A. S.; Yoon, Y.; Wuttig, A.; Surendranath, Y. Mesostructure-Induced Selectivity in CO_2 Reduction Catalysis. *J. Am. Chem. Soc.* **2015**, *137* (47), 14834−14837.
(69) Hansen, H. A.; Varley, J. B.; Peterson, A. A.; Nørskov, J. K. Understanding Trends in the Electrocatalytic Activity of Metals and Enzymes for CO_2 Reduction to CO. *J. Phys. Chem. Lett.* **2013**, *4* (3), 388−392.
(70) Peterson, A. A.; Abild-Pedersen, F.; Studt, F.; Rossmeisl, J.; Nørskov, J. K. How copper catalyzes the electroreduction of carbon dioxide into hydrocarbon fuels. *Energy Environ. Sci.* **2010**, *3* (9), 1311.
(71) Feng, Y.; An, W.; Wang, Z.; Wang, Y.; Men, Y.; Du, Y. Electrochemical CO_2 Reduction Reaction on M@Cu(211) Bimetallic Single-Atom Surface Alloys: Mechanism, Kinetics, and Catalyst Screening. *ACS Sustainable Chem. Eng.* **2020**, *8* (1), 210−222.
(72) Durand, W. J.; Peterson, A. A.; Studt, F.; Abild-Pedersen, F.; Nørskov, J. K. Structure effects on the energetics of the electrochemical reduction of CO_2 by copper surfaces. *Surf. Sci.* **2011**, *605* (15−16), 1354−1359.
(73) Liu, X.; Xiao, J.; Peng, H.; Hong, X.; Chan, K.; Nørskov, J. K. Understanding trends in electrochemical carbon dioxide reduction rates. *Nat. Commun.* **2017**, *8* (1), 15438.
(74) Kastlunger, G.; Lindgren, P.; Peterson, A. A. Controlled-Potential Simulation of Elementary Electrochemical Reactions: Proton Discharge on Metal Surfaces. *J. Phys. Chem. C* **2018**, *122* (24), 12771−12781.
(75) Sundararaman, R.; Goddard, W. A., III; Arias, T. A. Grand canonical electronic density-functional theory: Algorithms and applications to electrochemistry. *J. Chem. Phys.* **2017**, *146* (11), 114104.
(76) Hutchison, P.; Warburton, R. E.; Soudackov, A. V.; Hammes-Schiffer, S. Multicapacitor Approach to Interfacial Proton-Coupled Electron Transfer Thermodynamics at Constant Potential. *J. Phys. Chem. C* **2021**, *125* (40), 21891−21901.
(77) Gauthier, J. A.; Dickens, C. F.; Heenen, H. H.; Vijay, S.; Ringe, S.; Chan, K. Unified Approach to Implicit and Explicit Solvent Simulations of Electrochemical Reaction Energetics. *J. Chem. Theory Comput.* **2019**, *15* (12), 6895−6906.
(78) Hörmann, N. G.; Andreussi, O.; Marzari, N. Grand canonical simulations of electrochemical interfaces in implicit solvation models. *J. Chem. Phys.* **2019**, *150* (4), 041730.
(79) Pillai, H. S.; Xin, H. New Insights into Electrochemical Ammonia Oxidation on Pt(100) from First Principles. *Ind. Eng. Chem. Res.* **2019**, *58* (25), 10819−10828.
(80) Masood, Z.; Ge, Q. Comparative Study of Computational Hydrogen Electrodes and Constant Electrode Potential Models Applied to Electrochemical Reduction of CO_2 and Oxygen Evolution Reaction on Metal Oxides/Copper Catalysts. *J. Phys. Chem. C* **2023**, *127* (48), 23170−23179.
(81) Greeley, J.; Stephens, I. E. L.; Bondarenko, A. S.; Johansson, T. P.; Hansen, H. A.; Jaramillo, T. F.; Rossmeisl, J.; Chorkendorff, I.; Nørskov, J. K. Alloys of platinum and early transition metals as oxygen reduction electrocatalysts. *Nat. Chem.* **2009**, *1* (7), 552−556.
(82) Nie, X.; Esopi, M. R.; Janik, M. J.; Asthagiri, A. Selectivity of CO_2 Reduction on Copper Electrodes: The Role of the Kinetics of Elementary Steps. *Angew. Chem., Int. Ed.* **2013**, *52* (9), 2459−2462.
(83) Peterson, A. A.; Nørskov, J. K. Activity Descriptors for CO2 Electroreduction to Methane on Transition-Metal Catalysts. *J. Phys. Chem. Lett.* **2012**, *3* (2), 251−258.
(84) Wan, M.; Yang, Z.; Morgan, H.; Shi, J.; Shi, F.; Liu, M.; Wong, H. W.; Gu, Z.; Che, F. Enhanced CO_2 Reactive Capture and Conversion Using Aminothiolate Ligand−Metal Interface. *J. Am. Chem. Soc.* **2023**, *145* (48), 26038−26051.

(85) Chan, K.; Nørskov, J. K. Electrochemical Barriers Made Simple. *J. Phys. Chem. Lett.* **2015**, *6* (14), 2663−2668.
(86) Nørskov, J. K.; Rossmeisl, J.; Logadottir, A.; Lindqvist, L.; Kitchin, J. R.; Bligaard, T.; Jónsson, H. Origin of the Overpotential for Oxygen Reduction at a Fuel-Cell Cathode. *J. Phys. Chem. B* **2004**, *108* (46), 17886−17892.
(87) Ohio Supercomputer Center. 1987. https://www.osc.edu/about/mission (accessed Oct 25, 2024).

https://doi.org/10.1021/jacs.4c09744
J. Am. Chem. Soc. 2024, 146, 31633−31646